Continuous Planetary Polar Observation from Hybrid Pole-Sitters at Venus, Earth, and Mars

By Jeannette HEILIGERS[1, 2], Thomas D. van den OEVER[1], Matteo CERIOTTI[3], Patricia MULLIGAN[4], and Colin R. McINNES[3]

[1] *Faculty of Aerospace Engineering, Delft University of Technology, Delft, The Netherlands*
[2] *Colorado Center for Astrodynamics Research, Department of Aerospace Engineering Sciences, University of Colorado Boulder, Boulder, Colorado, USA*
[3] *Systems Power and Energy, School of Engineering, University of Glasgow, Glasgow, United Kingdom*
[4] *Annapolis, Maryland, USA*

(Received 1st Dec, 2016)

A pole-sitter is a satellite that is stationed along the polar axis of the Earth, or any other planet, to generate a continuous, hemispherical view of the planet's polar regions. In order to maintain such a vantage point, a low-thrust propulsion system is required to counterbalance the gravitational attraction of the planet and the Sun. Previous work has considered the use of solar electric propulsion (SEP) or a hybrid configuration of an SEP thruster and a solar sail to produce the required acceleration. By subsequently optimising the propellant consumption by the thruster, estimates of the mission performance in terms of the payload capacity and mission lifetime have been obtained. This paper builds on these results and aims at lifting the pole-sitter concept to the next level by extending the work both from a technical and conceptual perspective: from a technical perspective, this paper will further improve the mission performance by optimising the pole-sitter orbits for the payload capacity or mission lifetime instead of for the propellant consumption. The results show that, at Earth, this allows improvements in the order of 5-10 percent in terms of payload capacity and mission lifetime. Furthermore, on a conceptual level, this paper will, for the first time, investigate the possibility of so-called quasi-pole-sitter orbits. For quasi-pole-sitter orbits the requirement to be *exactly on* the polar axis is relaxed to allow some movement around the polar axis as long as continuous observation of the entire polar region at a desired minimum elevation angle is achieved. This ultimately enables solar sail-only pole-sitter orbits that are no longer limited in performance by the SEP propellant consumption. Finally, this paper extends all analyses to other inner Solar System planets, showing that Mars provides excellent conditions for a pole-sitter platform with its low mass and relatively far distance from the Sun. With this extension of the pole-sitter concept to other planets as well as considering, for the first time, the option of quasi-pole-sitter orbits, the concept is lifted to the next level, strengthening the feasibility and utility of these orbits for continuous planetary polar observation.

Key Words: Pole-sitter, Polar Observation, Trajectory Optimisation, Low-thrust propulsion, Solar Sailing

1. Introduction

The fixed geometry between geostationary satellites and the Earth enables continuous coverage of the equatorial zones and large parts of the temperate zones, allowing unique applications in the field of Earth observation and telecommuni-cations. However, due to the geostationary satellites' relatively close distance to Earth, their elevation angles at latitudes above 55 deg are not sufficient to assure a direct line-of-sight. Coverage of these regions can be achieved with low-altitude polar-orbiting satellites, which provide high spatial resolution observations, but poor temporal resolution as multiple passages are required to achieve uniform coverage. Higher temporal resolution can be achieved from other Keplerian orbits such as Molniya orbits, but, still, satisfactory coverage of the polar caps or high-latitude regions cannot always be achieved. When turning to non-Keplerian orbits, concepts such as Taranis orbits,[1)] solar sail displaced equilibria,[2)] and eight-shaped orbits[3)] in the Sun-Earth system have been proposed, all providing a different trade-off between spatial resolution and temporal resolution (in terms of number of spacecraft required for continuous coverage) as well as in the required propulsion technology. The concept of a pole-sitter adds to this trade-off: it proposes the use of a low-thrust propulsion system to maintain a satellite along the Earth's polar axis. As such, for an observer on the North (or South) Pole, the satellite would always be directly overhead, enabling polar observation capabilities with unprecedented temporal resolution. However, the magnitude of the required control acceleration is significant and to produce it with current or near-term technology the satellite would have to be placed at altitudes of the same order of magnitude as the distance to the Sun-Earth L_1 point. This does not necessarily limit the observational capabilities as demonstrated by the EPIC camera onboard NOAA/NASA's DSCOVR mission.[1] DSCOVR is orbiting the Sun-Earth L_1 point and provides near real-time images of the Sun-lit side of the Earth, showing what is feasible from such distances.

The concept of a pole-sitter has been under investigation for

[1] NASA/NOAA, DSCOVR::EPIC::Earth Polychromatic Camera, http://epic.gsfc.nasa.gov/, Accessed 4 November 2016

many years[4, 5] and results from previous studies have shown the performance of a pole-sitter mission for different propulsion configurations. While the pole-sitter can be maintained using only a solar electric propulsion (SEP) thruster ('pure-SEP configuration'), the mission performance (in terms of payload capacity or mission lifetime) can be significantly improved when complementing the thruster with a solar sail ('hybrid configuration'). As a propellant-less propulsion system,[6, 7] the solar sail lowers the demand on the SEP thruster, thereby significantly reducing the propellant consumption. Besides different propulsion configurations, also different orbit configurations have been considered, requiring the spacecraft to either maintain a constant altitude above the Earth or allowing it to change its separation from the Earth during the year. The latter enables a further reduction in the propellant consumption by the SEP thruster, thereby further increasing the available payload mass or extending the mission lifetime.

This paper will build on these results in many ways. First of all, all mission analysis work conducted in this field has so-far focused on minimising the propellant consumption by the SEP thruster. However, the true objective would be to maximise the payload mass and/or mission lifetime. This paper will therefore investigate these objective functions and demonstrate their impact on the orbit and mission performance. Secondly, this paper investigates the possibility of relaxing the requirement that the spacecraft has to maintain a position *exactly* along the polar axis and instead allowing a slight movement around the polar axis without compromising on the continuous view of the entire Arctic or Antarctic region. Finally, the paper will extend all these analyses to pole-sitters at other, inner Solar System planets.[8]

2. Dynamical system

Following previous work,[4, 5] the pole-sitter orbits are designed within the framework of the Sun-Earth circular restricted three-body problem (CR3BP),[9] using the Sun-Earth synodic reference frame, $A(\hat{\mathbf{x}},\hat{\mathbf{y}},\hat{\mathbf{z}})$, that is schematically presented in Fig. 1a: the x-axis points along the Sun-Earth line in the direction of the Earth, the z-axis is oriented perpendicular to the ecliptic plane and the y-axis completes the right-handed reference frame. Furthermore, the traditional system of canonical units is used, normalising the Sun-Earth distance, the frame's angular velocity, ω, and the Sun-Earth system mass to unity. Using the mass ratio, $\mu = m_E/(m_S+m_E) = 3.0404\times10^{-6}$ with m_S and m_E the masses of the Sun and Earth, respectively, the location of the Sun and Earth along the x-axis become $-\mu$ and $1-\mu$, respectively. The dynamics of the pole-sitter satellite in the CR3BP then become:

$$\ddot{\mathbf{r}} + 2\boldsymbol{\omega}\times\dot{\mathbf{r}} = \mathbf{a}_T + \mathbf{a}_s - \nabla U \tag{1}$$

In Eq. (1), $\mathbf{r} = [x \quad y \quad z]^T$ is the satellite's dimensionless position vector, $\boldsymbol{\omega} = \omega\hat{\mathbf{z}}$ is the synodic frame's angular velocity vector and $U = -\frac{1}{2}(x^2+y^2) - ([1-\mu]/r_1 + \mu/r_2)$ is the effective potential with the Sun-satellite and Earth-satellite position vectors defined as $\mathbf{r}_1 = [x+\mu \quad y \quad z]^T$ and $\mathbf{r}_2 = [x-(1-\mu) \quad y \quad z]^T$, respectively. Finally, $\mathbf{a}_T$ and $\mathbf{a}_s$ are the acceleration vectors produced by the SEP thruster and solar sail, respectively. Note that for the pure-SEP configuration, $\mathbf{a}_s = \mathbf{0}$.

To model the acceleration from the SEP thruster it is assumed that the thruster is steerable and can provide an adjustable thrust force. Furthermore, using a Cartesian representation to define the thrust vector, $\mathbf{T} = [T_x \quad T_y \quad T_z]^T$, the SEP acceleration vector can be written as:

$$\mathbf{a}_T = \frac{\mathbf{T}}{m} \tag{2}$$

Note that, due to the propellant consumption by the SEP thruster, the set of dynamical equations in Eq. (1) need to be complemented by an equation to account for the change in satellite mass, m:

$$\dot{m} = -T/(I_{sp}g_0) \tag{3}$$

with g_0 the Earth's standard gravity acceleration. For the thruster's specific impulse, I_{sp}, a value of 3200 s is conservatively assumed based on existing ion engine technology suitable for the mission under consideration (e.g., NSTAR/DS1[10], EADS/Astrium RIT-XT[11], or QinetiQ T6[12]).

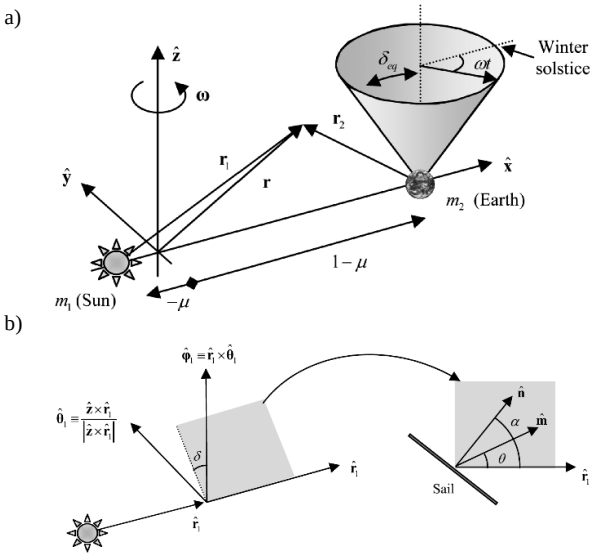

Fig. 1a) Definition of Sun-Earth CR3BP reference frame ('frame A') and polar axis conical motion.[4] b) Definition of reference 'frame B' and solar sail control angles.[4]

To model the solar sail acceleration, an non-ideal sail model is considered, that accounts for specular reflection and partial absorption of the solar photons:[6]

$$\mathbf{a}_s = \frac{1}{2}\beta_0\frac{m_0}{m}\frac{1-\mu}{r_1^2}\cos\alpha\left(g\cos\alpha\hat{\mathbf{n}}^{(A)} + h\sin\alpha\hat{\mathbf{t}}^{(A)}\right) \tag{4}$$

with β_0 the solar sail lightness number, which is a function of the sail area to spacecraft mass ratio. Near-term values for the lightness number are in the order of $\beta_0 = 0.05$ with a value of $\beta_0 = 0.1$ representing mid- to far-term technology.[13, 14] Furthermore, m_0 is the mass at the start of the pole-sitter mission, α is the cone angle of the sail (i.e., the angle between the Sun-direction and the normal to the solar sail), $\hat{\mathbf{n}}^{(A)}$ is the unit vector normal to the sail expressed in $A(\hat{\mathbf{x}},\hat{\mathbf{y}},\hat{\mathbf{z}})$, $\hat{\mathbf{t}}^{(A)}$ is the unit vector parallel to the sail expressed in $A(\hat{\mathbf{x}},\hat{\mathbf{y}},\hat{\mathbf{z}})$, and

g and h are reflectivity coefficients of the sail. For the computation of these reflectivity coefficients, it is important to note that part of the sail membrane is assumed to be covered with thin-film solar cells (TFSC) to produce power for the SEP thruster (in case of the pure-SEP configuration the use of solar panels will be assumed). These TFSC will have different optical properties than the sail, which is accounted for in the coefficients g and h through:

$$g = 1 + \tilde{r}_s + \frac{A_{TF}}{A}\left(\tilde{r}_{TF} - \tilde{r}_s\right),\ h = 1 - \tilde{r}_s - \frac{A_{TF}}{A}\left(\tilde{r}_{TF} - \tilde{r}_s\right) \quad (5)$$

where A and A_{TF} are the sail area and area of the sail covered with TFSC and $\tilde{r}_s$ = 0.9 and $\tilde{r}_{TF}$ = 0.4 are the reflectivity coefficients of the sail membrane and TFSC, respectively.[15)]

Finally, the unit vectors $\hat{\mathbf{n}}$ and $\hat{\mathbf{t}}$ can most easily be expressed in an auxiliary frame ('frame B', $B\left(\hat{\mathbf{r}}_1, \hat{\boldsymbol{\theta}}, \hat{\boldsymbol{\varphi}}\right)$), see Fig. 1b, which is defined with respect the CR3BP frame ('frame A') of Fig. 1a through:

$$\boldsymbol{\xi}^{(A)} = \left[\hat{\mathbf{r}}_1 \quad \hat{\boldsymbol{\theta}}_1 \quad \hat{\boldsymbol{\varphi}}_1\right]\boldsymbol{\xi}^{(B)} = \left[\frac{\mathbf{r}_1}{|\mathbf{r}_1|} \quad \frac{\hat{\mathbf{z}}\times\hat{\mathbf{r}}_1}{|\hat{\mathbf{z}}\times\hat{\mathbf{r}}_1|} \quad \hat{\mathbf{r}}_1\times\hat{\boldsymbol{\theta}}_1\right]\boldsymbol{\xi}^{(B)} \quad (6)$$

Then, using the definition of the cone angle, α, and clock angle, δ, as given in Fig. 1b, the normal vector to the sail can be expressed as:

$$\hat{\mathbf{n}}^{(B)} = \left[\cos\alpha \quad \sin\alpha\sin\delta \quad \sin\alpha\cos\delta\right]^T \quad (7)$$

Further details on the computation of all components required for Eq. (4) can be found in 4).

3. Orbital constraints

Due to the obliquity between the equatorial and ecliptic planes, δ_{eq} = 23.5 deg, the polar axis describes a clockwise conical motion in the synodic frame of the CR3BP, see Fig. 1a. A pole-sitter spacecraft would thus have to follow this apparent conical motion during the year where different scenarios can be envisaged:

- Constant altitude pole-sitter: the satellite maintains a constant separation, d, from the Earth. The instantaneous position of the pole-sitter spacecraft at time t is then given by:

$$\mathbf{r}(t) = \begin{bmatrix} d\sin\delta_{eq}\cos\omega t + (1-\mu) \\ -d\sin\delta_{eq}\sin\omega t \\ d\cos\delta_{eq} \end{bmatrix} \quad (8)$$

- Variable altitude pole-sitter: the satellite maintains a position along the polar axis, but the separation from Earth is allowed to vary during the year. The variable d in Eq. (8) then becomes time dependent, $d(t)$.
- Quasi-pole-sitter: in this scenario the pole-sitter constraint is relaxed, allowing the spacecraft to move around the polar axis as long as any location above a certain latitude, $\delta_{\min}$, can be observed continuously at a minimum elevation angle, $\varepsilon_{\min}$. This constraint is visualised in Fig. 2a and can be expressed as:

$$\phi = \cos^{-1}\left(\hat{\mathbf{p}}\cdot\hat{\mathbf{r}}_3\right) \le \phi_{\max} = \delta_{\min} - \varepsilon_{\min} \quad (9)$$

with

$$\mathbf{p}(t) = \begin{bmatrix} \sin\delta_{eq}\cos\omega t \\ -\sin\delta_{eq}\sin\omega t \\ \cos\delta_{eq} \end{bmatrix},\ \hat{\mathbf{r}}_3 = \frac{\mathbf{r}_2 - \begin{bmatrix}0 & 0 & h_p\end{bmatrix}^T}{\left|\mathbf{r}_2 - \begin{bmatrix}0 & 0 & h_p\end{bmatrix}^T\right|} \quad (10)$$

In Eq. (10), h_p can be computed from the law of sines:

$$h_p = \frac{\sin\left(90^o + \varepsilon_{\min}\right)}{\sin\left(\delta_{\min} - \varepsilon_{\min}\right)} r_E \quad (11)$$

with r_E the Earth's radius. The blue cones in Fig. 2b (superimposed on the polar axis cone) show the allowable motion around the polar axis at four epochs during the year (at winter, spring, summer and autumn) and for a minimum elevation angle of 60 deg for the entire Arctic circle, i.e., $\varepsilon_{\min}$ = 60 deg and $\delta_{\min}$ = 65.8 deg.

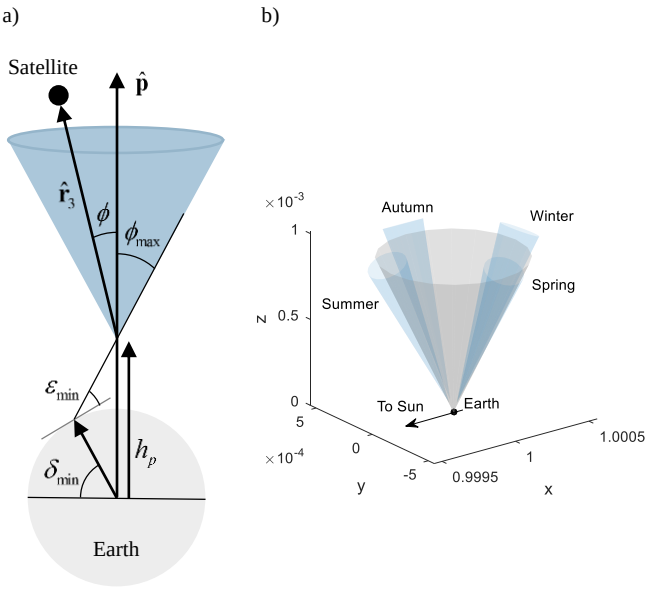

Fig. 2a) Schematic quasi-pole-sitter constraint. b) Allowable deviation from polar axis during winter, spring, summer and autumn for $\varepsilon_{\min}$ = 60 deg.

4. Spacecraft mass budget

In order to compute the lifetime of the mission or the payload mass that can be carried onboard, a spacecraft mass budget is used similar to the one proposed in 5, 14):

$$m_0 = \left(m_{prop} + m_{tank} + m_{thr} + m_{other}\right)\left[1 + \varepsilon_{old}\right] + m_{pay} + \begin{cases} m_{SA}\left[1+\varepsilon_{old}\right] & \text{SEP} \\ \left(m_{rad}+m_g\right)\left[1+\varepsilon_{old}\right] + \left(m_s + m_{TF}\right)\left[1+\varepsilon_{new}\right] & \text{Hybrid} \end{cases} \quad (12)$$

In Eq. (12), the subscripts '*prop*', '*tank*', '*thr*', '*other*', '*pay*', '*SA*', '*rad*', '*g*', '*s*', and '*TF*' refer to the propellant, the propellant tanks, the SEP thruster, other subsystems, payload, solar arrays, radiator, gimbal, solar sail, and thin-film solar cells, respectively. The equation furthermore shows that the pure-SEP and hybrid configurations have some subsystems in common, while other subsystems are unique to one of the two configurations. For example, the hybrid configuration includes

radiators to dissipate excess power produced by the TFSC. This is required because the attitude of the TFSC with respect to the Sun is constrained by the attitude of the solar sail. The TFSC may therefore produce more power than required by the SEP thruster. The mass budget also accounts for margins, using a small margin, ε_{old} = 0.05, for existing and flight-proven technologies and a larger margin, ε_{new} = 0.2, for new technologies.

Further details on how each mass subsystem is to be computed are omitted in this paper for brevity and can be found in 5, 14). The only detail of importance throughout the rest of this paper is the fact that the SEP thruster mass (and therefore also the gimbal mass) as well as the solar array/TFSC mass depend on the maximum thrust required from the thruster during the pole-sitter's mission lifetime.

5. Optimisation algorithm

The objective of this paper is to find optimal pole-sitter orbits, where 'optimal' can be defined as:

- Minimum SEP propellant consumption
- Maximum payload capacity for a fixed mission lifetime (1 year in this paper)
- Maximum mission lifetime for a fixed payload mass (100 kg in this paper).

Note that the payload capacity for a multi-year mission and the mission lifetime are computed by assuming a fixed propellant mass fraction for each year: i.e., the orbit is optimised over 1 year (i.e., one orbit revolution) and the resulting propellant mass fraction is used to compute the propellant consumption in subsequent years. The lifetime of the mission is defined as the moment all SEP propellant has been consumed.

Also note that these objective functions are not the same, i.e., a minimum propellant usage does not automatically allow the maximum payload capacity. This is strongly related to the maximum thrust applied throughout the trajectory and can be demonstrated with a simple example. Assume a trajectory where three options are available:

- No peak thrust is included. This will have no effect on the thruster mass or the yearly propellant consumption.
- A moderate peak thrust is applied, which will increase the thruster mass by 3 kg and reduces the average yearly propellant consumption by 1 kg.
- A large peak thrust is applied, which increases the thruster mass by 20 kg and reduces the average yearly propellant consumption by 2 kg.

The best choice for each objective function can be justified as follows:

- Minimum SEP propellant usage: it is best to apply the large peak thrust, because it provides the largest reduction in the propellant mass. The effect on the thruster mass is not relevant for this objective.
- Maximum payload capacity for a 1 year mission: regardless of whether a moderate or a large peak thrust is applied, the reduction in propellant consumption after one year does not outweigh the increase in thruster mass. It is therefore best not to include any peak thrust.
- Maximum lifetime for a 100 kg payload: in this case the choice depends on the actual lifetime of the mission. If the lifetime is in the order of 4 years, then the moderate peak thrust will be optimal as the reduction in propellant consumption over 4 years outweighs the increase in thruster mass. For longer mission lifetimes (> 10 years) the peak thrust may be most optimal.

With the different objective functions defined, the actual approach and algorithm used to find optimal pole-sitter orbits depends on the orbital constraints imposed, i.e., whether the constant altitude, variable altitude or quasi-pole-sitter is considered. In the case of the constant altitude pole-sitter, the trajectory is fully defined through Eq. (8), allowing the equations of motion to be inverted to find the controls required to follow that trajectory. In the case of the pure-SEP configuration, the algorithm ends there because the controls cannot be optimised as the SEP thruster simply has to provide whatever the inversion of the dynamics demands. As such, the required thrust at each point along the trajectory can be obtained from simple algebraic operations only. Instead, for the hybrid configuration, the solar sail can provide part of the required control and the problem becomes to determine the attitude of the sail at each point in the trajectory that optimises one of the three previously defined objectives. This requires the solution to a nonlinear programming (NLP) problem, which can be obtained numerically, for example by using the interior-point algorithm implemented in the MATLAB® function *fmincon.m*. More details on this approach can be found in 4).

When considering the variable altitude pole-sitter and the quasi-pole-sitter, the trajectory is no longer predefined and will have to be optimised simultaneously with the controls. To this end, a direct multiple shooting (DMS) algorithm[16, 17] is implemented. The algorithm discretises the trajectory into a finite number of nodes, N, thereby splitting the trajectory into $N-1$ segments. The state vector at each node i, $\mathbf{x}_i = \begin{bmatrix}\mathbf{r} & \dot{\mathbf{r}} & m\end{bmatrix}^T$ and the controls ($\mathbf{u}_i = \begin{bmatrix}T_x & T_y & T_z\end{bmatrix}^T$ for the pure-SEP configuration or $\mathbf{u}_i = \begin{bmatrix}T_x & T_y & T_z & \alpha & \delta\end{bmatrix}^T$ for the hybrid configuration) form the decision vector. The dynamics in Eq. (1) are forward integrated from node i to node $i+1$ (except for the final node) using the state vector $\mathbf{x}_i$ as initial condition. Subsequently, constraints are imposed to ensure that:

- The state vector at the end of segment n equals the state vector at the start of the next segment, $n+1$
- The first and last nodes coincide in terms of position and velocity states to ensure periodicity of the orbits, $\mathbf{x}_1 = \mathbf{x}_N$
- The initial mass (i.e., on the first node) is 1000 kg, m_0 = 1000 kg
- The maximum cone angle of the sail is set to 90 deg to prevent the optimisation algorithm of using a solar sail acceleration component in the direction of the Sun which the sail is unable to generate[6)]

The resulting NLP problem is once again solved with the interior-point algorithm implemented in the MATLAB® function *fmincon.m* using N = 15 nodes. Furthermore, initially, the controls will be assumed to be constant across the segments (implying discontinuities in the control profiles across the nodes). Later on in this paper, more refined control profiles across the segments will be investigated, but the results will show that this refinement has very limited influence on the objective function values. Finally, regarding the initial guess to

initialise the optimisation algorithm, two main approaches are applied:

1) The analytically defined constant altitude SEP orbit is used as initial guess for the variable altitude pole-sitter orbit, which in its turn is used to initiate the optimisation of the quasi-pole-sitter orbit.
2) A continuation on β_0 is applied, using the result for a smaller value for β_0 as initial guess for the optimisation of a pole-sitter orbit with a slightly larger value for β_0.

6. Propellant-optimal pole-sitter orbits

6.1 One-year pole-sitter orbits

The results for the first objective function, i.e., minimum SEP propellant consumption, are provided in Fig. 3. The figures in subplots a-d) provide the optimal trajectories for a constant altitude, variable altitude and quasi-pole-sitter (both $\varepsilon_{\min} = 30$ deg and $\varepsilon_{\min} = 60$ deg) for both the pure-SEP configuration ($\beta_0 = 0$) and the previously established near- and far-term lightness numbers, $\beta_0 = 0.05$ and $\beta_0 = 0.1$. The results for the constant and variable altitude pole-sitters are in good agreement with previously found results,[4, 8] thereby validating the optimisation algorithm. When considering the results for the quasi-pole-sitter orbits, and in particular for the pure-SEP configuration, slightly elliptic orbits are obtained that lie inside the grey polar axis cone during winter and summer, but outside the grey cone at the spring and autumn equinoxes. For the hybrid configuration the orbit mainly shifts towards the Sun both in winter and summer. The actual propellant consumption for both a 1 year and 5 year mission is provided in Fig. 3e, where the results for the 5 year mission are extrapolated from the 1 year mission. The latter shows that the propellant mass decreases for increasing sail lightness numbers with the remarkable result of zero propellant consumption for the quasi-pole-sitters with $\varepsilon_{\min} = 30$ deg and $\beta_0 \geq 0.06$. This result indicates that the pole-sitter orbits can be maintained using *only* a solar sail if an elevation angle of 30 deg across the entire Arctic circle is sufficient to fulfill the mission objectives. Note that for the case that the pole-sitter can be maintained using only a solar sail, the objective function is changed from minimising the propellant consumption to minimising the Earth-satellite distance to maximise the spatial resolution of the observations.

6.2 Multiple year orbits

When computing the propellant consumption for the 5-year mission in Fig. 3e it is assumed that both the orbit and the propellant mass fraction remain unchanged from one year to the next. However, clearly, after one year the spacecraft has consumed propellant, thereby effectively increasing the sail's lightness number at the start of the second orbit revolution. This increases the contribution of the sail to the required acceleration, which may allow for a different, more optimal orbit to be flown during the second and any consecutive year. The effect of optimising the orbit over multiple years is investigated in this section for a particular case: the variable altitude pole-sitter for a hybrid configuration with $\beta_0 = 0.05$. The optimiser is still required to find a periodic orbit (i.e., the initial and final state vectors of the orbit must coincide), only now periodic is defined after 2 or 4 years/revolutions. Furthermore, the number of nodes in the DMS scheme are linearly increased with the number of years, i.e., 30 and 60 nodes for a mission of 2 and 4 years, respectively.

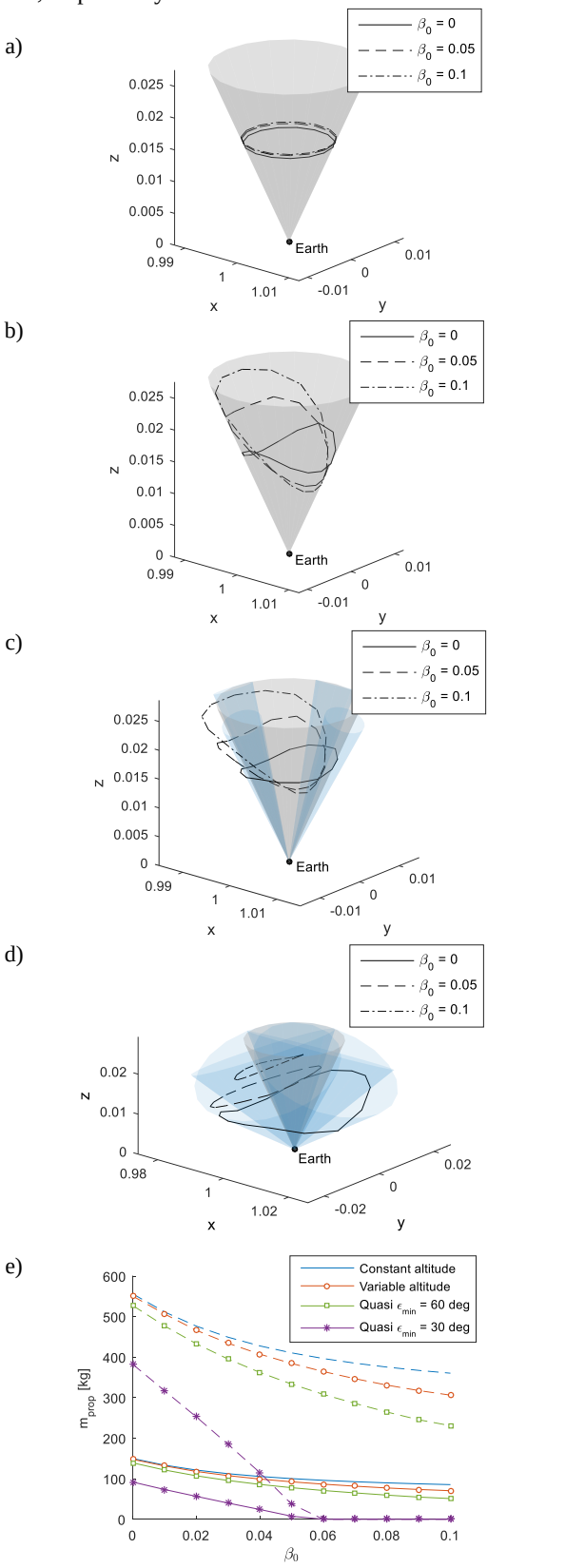

Fig. 3 Propellant-optimal pole-sitter orbits for different sail lightness numbers, β_0. a) Constant altitude pole-sitters. b) Variable altitude pole-sitters. c-d) Quasi-pole-sitters with $\varepsilon_{\min}$ = 60 deg (c) and $\varepsilon_{\min}$ = 30 deg (d). e) Propellant mass for a 1 year (solid lines) and 5 year (dashed line) mission.

The results are shown in Fig. 4 and Table 1. The orbital plots in Fig. 4 clearly show a change in the orbital evolution over the years, indicating that a repeat of the 1-year optimal orbit as shown in Fig. 3b is sub-optimal. Instead, the orbit becomes increasingly inclined over the years, which is in agreement with what was found in Fig. 3b: the larger the lightness number, the more inclined the orbit. The numerical values in Table 1 show that the consumed propellant after the first year is very similar whether the orbit is optimised over 1, 2, or 4 years and that the difference between the optimisations starts to appear after 2 years, where the 2- and 4-year orbits allow a mass saving of approximately 3 kg. This mass saving with respect to a repetition of the 1 year optimal orbit increases further to 4.7 and 13.7 kg after 4 years. These results thus show that a gain can be obtained from optimising the orbit over multiple years. However, this is a time-consuming process due to the significant increase in number of nodes (and therefore decision variables). The remainder of the paper will therefore assume the strategy of assuming a constant propellant mass fraction over the years. This will thus result in a conservative estimate of the actual propellant consumption.

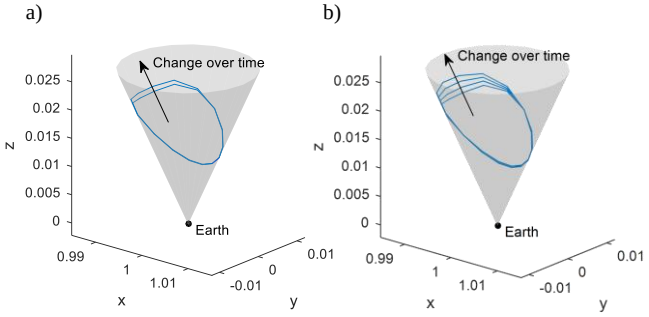

Fig. 4 Propellant-optimal variable altitude pole-sitter orbit for β_0 = 0.05 optimised over 2 years (a) and 4 years (b).

Table 1 Propellant consumption after 1, 2, or 4 years for optimising the orbit over different mission lifetimes.

	Propellant consumption after		
Optimised mission time	1 year	2 years	4 years
1 year	92.5	176.4	321.8
2 years	92.4	173.6	317.1
4 years	92.3	173.4	308.1

6.3 Effect of optimisation settings

The results in the previous sections have been produced under the assumption of constant controls along each of the 15 trajectory segments in the DMS scheme. However, more optimal results can be expected when increasing the number of nodes or considering more refined control representations, e.g., a polynomial control profile. The effect of these design choices will be investigated in this section for the same test case as used in Section 6.2: the variable altitude pole-sitter for a hybrid configuration with $\beta_0 = 0.05$.

First, the effect of doubling the number of nodes is provided in Fig. 5. This figure shows that the refined solution corresponds well to the 15-node solution, smoothening it in some places and oscillating around the 15-node solution in other places. However, the effect on the actual propellant consumption after one year is almost negligible: 92.492 kg and 92.468 kg for the 15-node and 30-node solution, respectively. The use of 15 nodes throughout the remainder of this paper is therefore justified as it significantly reduces the computational effort.

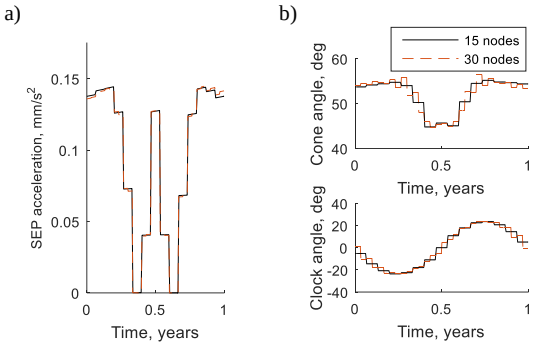

Fig. 5 Effect on controls by doubling the number of nodes. a) SEP acceleration. b) Solar sail control angles.

To investigate the effect of the assumption of constant controls along the DMS segments, the trajectory is also optimised assuming the following polynomial control representation:

$$u_{k,i}(t) = a_{k,i} + b_{k,i}t + c_{k,i}t^2 + d_{k,i}t^3 \tag{13}$$

where the subscripts k and i indicate that, for every control k (i.e., the three SEP thrust components and the sail's cone and clock angles) on each segment i, a different polynomial $u_{k,i}$ is used. The result of the polynomial representation is given by the red dashed lines in Fig. 6. The additional results in Fig. 6 are for further constraining the polynomial control presentation: 'polynomial continuous' indicates that the controls are continuous in value at the nodes whereas 'polynomial continuous derivative' indicates that both the value and derivative of the controls are continuous at the nodes. Fig. 6 shows that, the stricter the constraints imposed, the smoother the control profiles, but also the larger the propellant consumption. While an initial gain in propellant consumption is achieved from switching from constant to polynomial controls (92.492 kg and 92.223 kg, respectively) the propellant consumption increases slightly for polynomial 'continuous' and 'continuous derivative' controls (92.261 kg and 92.318 kg, respectively). The difference in propellant consumption between constant and fully constrained polynomial controls is thus only 0.178 kg (or 0.2 percent). The use of constant controls throughout the remainder of this paper can therefore be justified as it again significantly reduces the computational effort.

7. Payload- and lifetime-optimal pole-sitter orbits

With the results for the propellant-optimal pole-sitters obtained in the previous section and the analysis on the sensitivity of the results on the settings of the optimisation algorithm completed, further results for different objective functions can be produced. Note that to limit the number of results presented, only the variable altitude pole-sitter will be considered in this section.

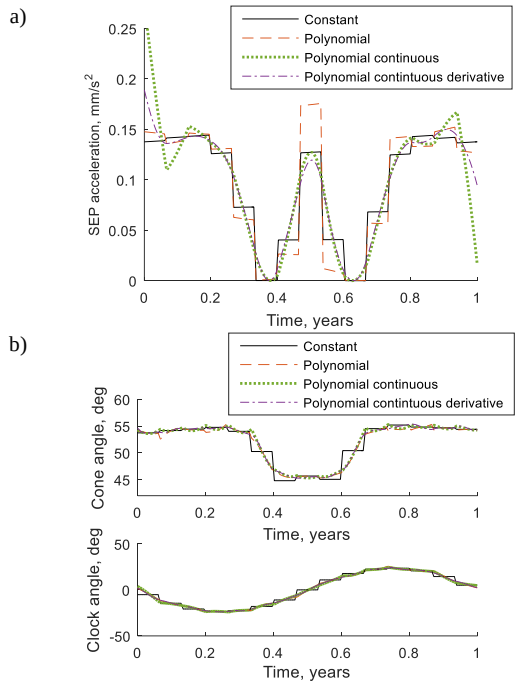

Fig. 6 Effect of polynomial representation of controls. a) SEP acceleration. b) Solar sail control angles.

As mentioned in Section 5, minimising the propellant mass does not consider the actual mass of the different subsystems and may therefore not be optimal when considering the available payload mass or achievable mission lifetime. For example, peaks in the thrust profile may occur which are beneficial from a propellant consumption point of view, but will require a relatively heavy thruster system; or, unfavourable solar sail angles may occur that require an unnecessarily large area of thin-film solar cells. To account for these, and other, effects, this section provides the results when optimising the pole-sitter orbit for the payload mass (for a fixed lifetime of 1 year, extrapolating the results to a mission of 5 years) or the lifetime (for a fixed payload mass of 100 kg) and compares these results with the previously obtained results for minimising the propellant mass. A summary of the results is presented in Fig. 7. Subplot a) provides the propellant mass for each of the objective functions (where the results for the optimal lifetime are rescaled to a 1- or 5-year mission), while subplots b) and c) provide the payload mass and lifetime for each of the objectives. Clearly, the objective corresponding to the label on the vertical axis of each of the subplots should provide the best result in that graph: for example, Fig. 7b correctly shows that the red line with round markers, which represents the maximum payload solution is on top for both a 1-year and 5-year mission. A similar reasoning should hold for Fig. 7a and b and in general this is true. However, the optimisation problem exhibits many local minima, which is dealt with by considering multiple different initial guesses (other than the systematic approaches outlined in Section 5) in order to produce the results in Fig. 7. However, as the figure shows, the use of different initial guesses still does not provide a guarantee that the global minimum is found or that the result does not converge to the initial guess, especially when the performance between different objective functions is only small. Further numerical details for the case of $\beta_0 = 0.05$ are provided in Table 2 and Fig. 8. The figure shows the subsystem mass components for the three different objective functions assuming either a 100 kg payload mass (Fig. 8a) or a mission lifetime of 1 year (Fig. 8b). From the figure it can be concluded that the results are very similar for the minimum propellant and maximum lifetime objectives. For the maximum payload mass a clear increase in the propellant mass can be observed, but this increase is offset by a much smaller thruster mass and zero radiator mass.

Finally, the plots in Fig. 7b) and c) show a sharp increase in the payload mass or lifetime between the pure-SEP option ($\beta_0 = 0$) and the hybrid configuration with $\beta_0 = 0.01$. To provide an explanation for this phenomenon, Fig. 9 is included, which shows the spacecraft subsystem mass breakdown for $\beta_0 = 0$ and $\beta_0 = 0.01$ and for the minimum propellant objective. As the figure shows, the gain in mission performance can be explained by a significant decrease in the power-supply subsystem mass when replacing solar panels by TFSC when switching between the pure-SEP and hybrid configurations, respectively.

Table 2 Objective function values for variable altitude pole-sitter orbits with $\beta_0 = 0.05$.

Objective	Propellant after 1 year, kg	Payload for 1 year mission, kg	Lifetime for 100 kg payload, Earth years
Minimum propellant	**321.7**	285.0	**3.9**
Maximum payload	392.8	**310.8**	3.7
Maximum lifetime	321.9	286.3	**3.9**

8. Pole-sitters at Venus and Mars

So far only pole-sitter orbits at Earth have been considered. However, the pole-sitter mission concept can also offer unique observation and communication opportunities at other inner Solar System planets. Therefore, this section will present a summary of the results for pole-sitters at Venus and Mars in a format very similar to the results for Earth. Details on the planetary parameters for Venus and Mars can be found in Table 3.

Starting with the propellant-optimal pole-sitters, Fig. 10a and b provide the orbital plots for the quasi-pole-sitters with ε_{min} = 60 deg and ε_{min} = 30 deg, respectively. The results for the constant altitude and variable altitude pole-sitters are omitted for brevity as they can also be found in 8). Note however that the propellant consumption for the constant and variable altitude pole-sitters at Venus are very similar, see Fig. 10c. This is due to the very small obliquity of the equator of Venus (and therefore very narrow pole-sitter cone), which does not allow for much variation in the dynamics along the pole-sitter orbit. Also note that Venus has an obliquity of -177.36 deg. The pole-sitter orbits shown in Fig. 10a and b are therefore above Venus' South Pole. Finally, also note that for a fair comparison with the results for the Earth the same value is assumed for the minimum latitude, δ_{min} = 65.8 deg, above which continuous coverage needs to be achieved. The effect of the quasi-pole-sitter constraint on the shape of the orbits is very similar as observed for pole-sitters at Earth, i.e., a shift towards the Sun. However, from the actual propellant consumption for all orbit types and for a range of lightness numbers in Fig. 10c and d it

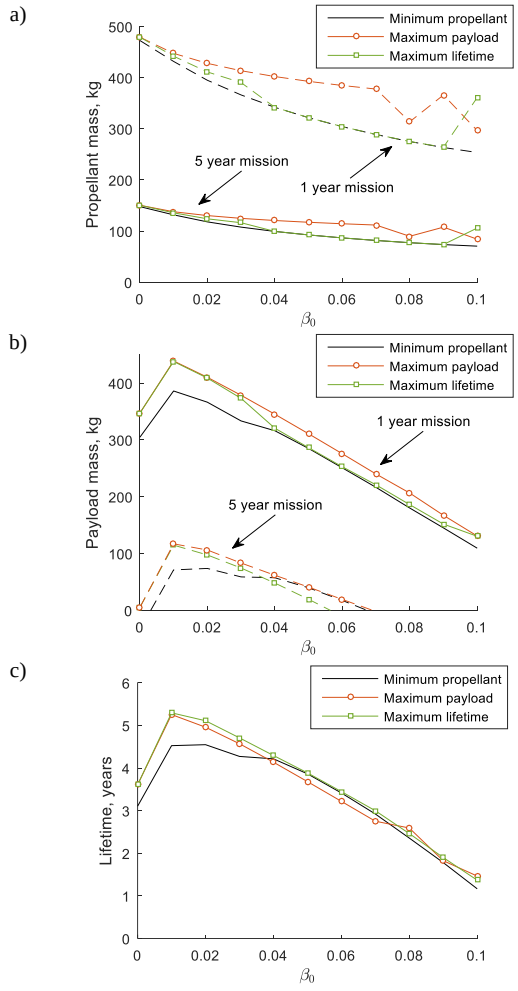

Fig. 7 Optimal variable altitude pole-sitter orbits optimised for the propellant consumption, payload capacity or mission lifetime.

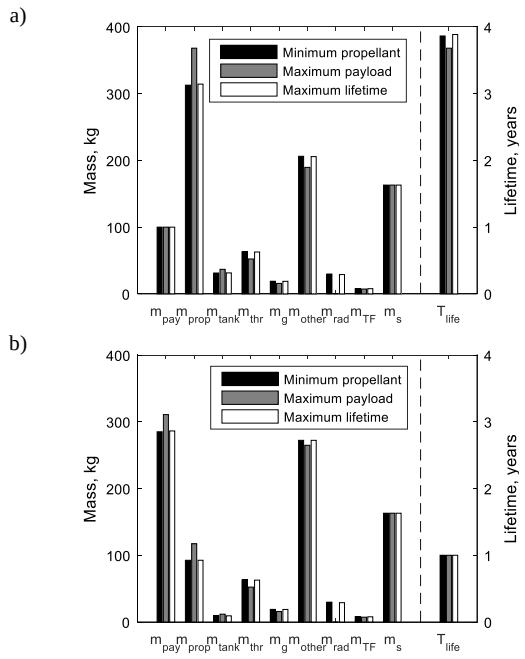

Fig. 8 Mass budget breakdown and mission lifetime for hybrid configuration with β_0 = 0.05. a) 100 kg payload mass. b) 1 year mission lifetime.

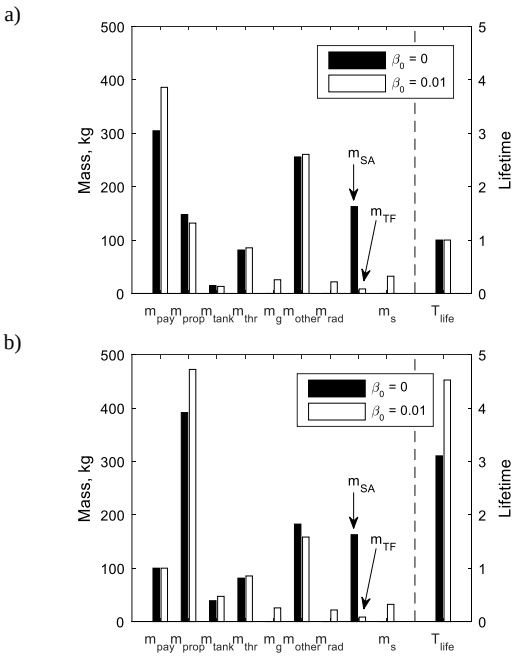

Fig. 9 Mass budget breakdown and mission lifetime for pure-SEP (β_0 = 0) and hybrid (β_0 = 0.01) configurations for minimum propellant pole-sitters. a) 100 kg payload mass. b) 1 year mission lifetime.

Table 3 Planetary parameters

	Venus	Earth	Mars
Planet mass, 10^{24} kg	4.8675	5.9723	0.64171
Planet radius, km	6049.8	6378.16	3389.5
Obliquity of equator, deg	-177.36	23.5	25.19
Solar irradiance at planet, W/m^2	2601.3	1367.0	586.2

can be concluded that the Venusian pole-sitters require more propellant than the pole-sitter at Earth, while the Martian pole-sitters require much less propellant (especially when considering that the propellant consumptions in Fig. 10c and d are for the shorter Venusian year and longer Martian year). Furthermore, similar to the Earth, solar sail-only quasi-pole-sitters exist for ε_{min} = 30 deg at both Venus and at Mars, although at Mars they exist at smaller lightness numbers than at Venus or Earth ($\beta_0 \geq 0.03$). Finally, when comparing the maximum distance from Venus and Mars along the orbit with the maximum distance for the pole-sitters at Earth, see Fig. 11, it can be concluded that Venusian and Martian pole-sitters exist much closer to the planet (approximately 750,000–1,500,00 km close), allowing a higher spatial resolution of the observations.

As for the pole-sitter orbits at Earth, it can be investigated if the pole-sitters at Venus and Mars could benefit from a change in objective function. Again, for brevity, only a particular case is investigated: the variable altitude pole-sitter with β_0 = 0.05. The results can be found in Table 4. For each objective function, the propellant consumption during the first year, the available payload for a 1-year mission and the achievable lifetime for a 100 kg payload mass is provided. The bold numbers indicate the best performance in that column, showing that the best propellant consumption, payload capacity and lifetime are achieved when optimising for those objectives, although the optimisation for the payload mass and lifetime for pole-sitters at Venus converged to the same solution. While for Venus both

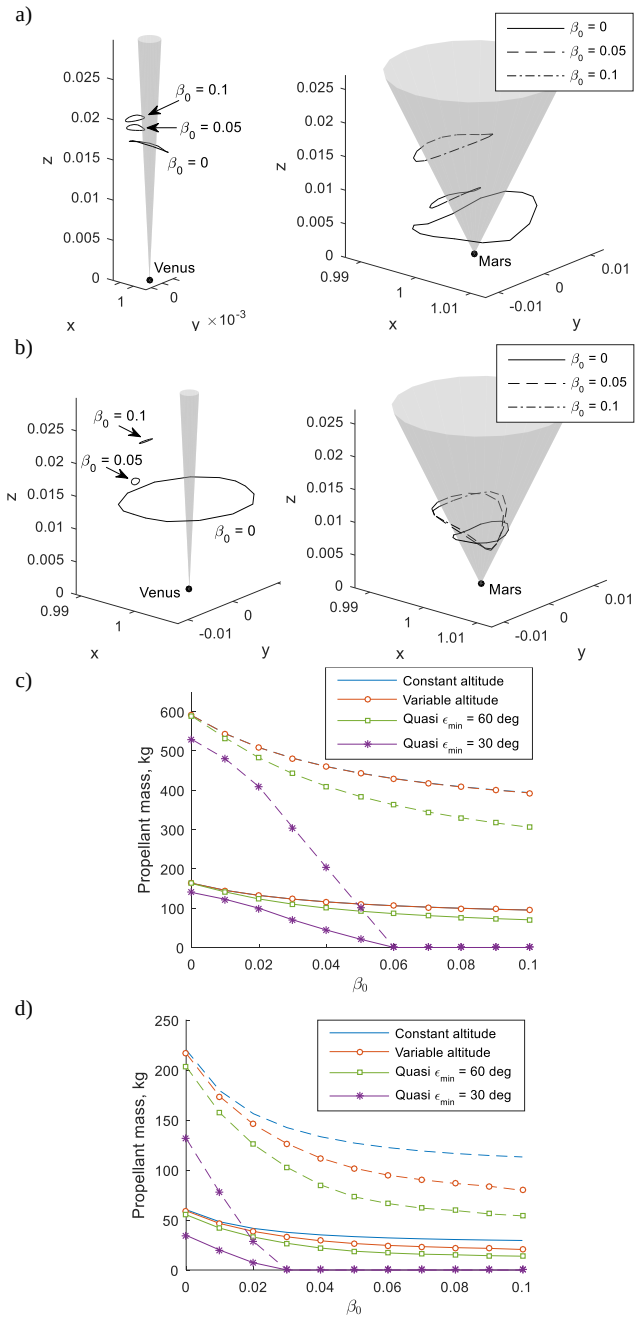

Fig. 10 Propellant-optimal pole-sitter orbits at Venus and Mars for different sail lightness numbers, β_0. a-b) Quasi-pole-sitters with ε_{min} = 60 deg (a) and ε_{min} = 30 deg (b). c-d) Propellant mass for 1 Venusian (c) or Martian (d) year (solid lines) and 5 Venusian (c) or Martian (d) years (dashed line).

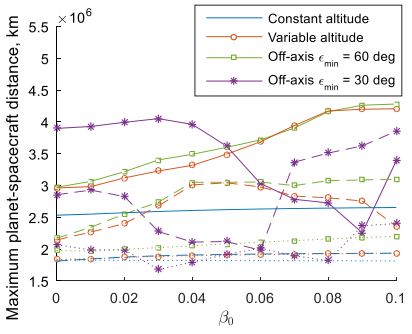

Fig. 11 Maximum planet-spacecraft distance for propellant-optimal pole-sitters for different sail lightness numbers, β_0. Solid, dotted, and dashed lines are for pole-sitters at Earth, Venus, and Mars, respectively.

Table 4 Optimised variable altitude pole-sitter orbits at Venus and Mars for β_0 = 0.05. *year refers to a Venusian/Martian year

Objective	Propellant after 1 year*, kg		Payload for 1 year* mission, kg		Lifetime for 100 kg payload, years*	
	Venus	Mars	Venus	Mars	Venus	Mars
Minimum propellant	**110.5**	**26.5**	256.0	437.2	3.0	20.8
Maximum payload	111.4	26.7	**278.6**	**440.5**	**3.3**	**20.9**
Maximum lifetime	111.4	26.5	**278.6**	428.9	**3.3**	**20.9**

the payload capacity and mission lifetime can be increased by approximately 9-10 percent, the gains for pole-sitters at Mars are negligible (less than a percent).

9. Utility of pole-sitters

The ability of the pole-sitter concept to observe the entire Arctic region (and similar regions at Mars and Venus) with unprecedented temporal resolution opens up a wide range of novel space applications. For example, continuous observations of the high-latitudes of the Earth will be crucial in on-going studies of global climate change, but also to support telecommunications, weather forecasting and ship navigation for the exploration and sustainable development of these regions. The polar region is of significant interest as it is projected to hold 30 percent of the world's undiscovered gas and 13 percent of the world's undiscovered oil.[18] In addition, with the northern sea routes opening up, an increase in shipping activity can be expected. Furthermore, continuous observation of the high-latitudes of the Earth is of importance for space weather monitoring and forecasting activities. For example, a continuous view of the *entire* aurora oval will allow observations of the direct response of the magnetosphere to changes in the solar wind, which will be critical to understanding the solar wind-magnetosphere coupling. It will also allow the detection and imaging of rarely observed phenomena such as transpolar arcs and cusp spots[19] to further the understanding of the cause for (and relation between) these phenomena. Finally, the polar regions are key in reaching out to the public to raise awareness and gain support for sustainable development. The DSCOVR mission is already providing us with an unprecedented near-live view of the Sun-lit hemisphere of the Earth. A similar image, but then of the polar regions, can be provided by the pole-sitter.

Pole-sitter utility for meeting communication and remote sensing requirements of several US government agencies including NOAA, NASA, USAF and NSF have been studied, often focusing on simultaneous satisfaction of multiple agency needs in one mission.[20-24] These applications have included the space weather, climate, and Arctic imagery cited above but other uses as well. Pole-sitters could permit hemispheric visibility for lunar communication, as well high volume data relay from the Earth's South Pole. Satellite to satellite communication could permit the essentially real time relay of low Earth orbiting meteorological satellites significantly improving their data latency while simultaneously simplifying those satellites' ground systems. The benign duty stations of pole-sitters, far from the

Earth's magnetic field and holding a constant position relative to the Sun with frequent lunar views have advantages for inter-satellite calibration, and simplified mission and sensor designs.

Further, what is true for the Earth/moon system holds for other planetary systems as well.

10. Conclusion

This paper has extended previous work carried out on the concept of a pole-sitter mission. In particular, the possibility of relaxing the pole-sitter constraint and allowing some movement around the polar axis has been investigated. The effect of this degree of freedom is a significant reduction in propellant consumption, even allowing solar sail-only pole-sitter orbits when requiring continuous observation of the entire Arctic circle (latitudes above 65.8 deg) at a minimum elevation angle of 30 deg. At Earth and Venus these solar sail-only pole-sitters can be achieved for solar sail lightness numbers larger than 0.06, while at Mars they already exist for smaller lightness numbers of 0.03. Additional investigations have focused on changing the objective function from minimising the propellant consumption to maximising the payload capacity or mission lifetime. For pole-sitters at Earth and Venus maximising the payload capacity shows a 9 percent increase in payload mass. While maximising the lifetime does not provide much improvement for pole-sitters at Earth, a 10 percent longer lifetime can be obtained for pole-sitters at Venus. While such improvements have not been observed for pole-sitters at Mars, Mars still provides an attractive mission scenario due to its far distance from the Sun and low mass: lifetimes of 20 Martian years, i.e., ~ 40 Earth years (10 times that of the lifetime of a pole-sitter at Earth), can be achieved for a 1000 kg spacecraft with a payload mass of 100 kg.

Acknowledgments

Colin McInnes acknowledges support through a Royal Society Wolfson Research Merit Award (2015-2020). Jeannette Heiligers acknowledges support of the Marie Skłodowska-Curie Individual Fellowship 658645 - S4ILS: Solar Sailing for Space Situational Awareness in the Lunar System.

References

1. Anderson, P. and Macdonald, M., "Extension of Highly Elliptical Earth Orbits Using Continuous Low-Thrust Propulsion," *Journal of Guidance, Control, and Dynamics*; Vol. 36, No. 1, 2013, pp. 282-292. doi: 10.2514/1.55304
2. Waters, T.J. and McInnes, C.R., "Periodic Orbits Above the Ecliptic in the Solar-Sail Restricted Three-Body Problem," *Journal of Guidance, Control, and Dynamics*; Vol. 30, No. 3, 2007, pp. 687-693. doi: 10.2514/1.26232
3. Ceriotti, M. and McInnes, C., "Natural and sail-displaced doubly-symmetric Lagrange point orbits for polar coverage," *Celestial Mechanics and Dynamical Astronomy*; Vol., 2012. doi: 10.1007/s10569-012-9422-2
4. Ceriotti, M. and McInnes, C.R., "Generation of Optimal Trajectories for Earth Hybrid Pole Sitters," *Journal of Guidance, Control, and Dynamics*; Vol. 34, No. 3, 2011, pp. 847-859. doi: 10.2514/1.50935
5. Ceriotti, M., Heiligers, J., and McInnes, C.R., "Trajectory and Spacecraft Design for a Pole-Sitter Mission," *Journal of Spacecraft and Rockets*; Vol. 51, No. 1, 2014, pp. 311-326. doi: 10.2514/1.A32477
6. McInnes, C.R., "Solar Sailing: Technology, Dynamics and Mission Applications," *Springer-Praxis Books in Astronautical Engineering*, Springer-Verlag, Berlin, 1999.
7. Vulpetti, G., Johnson, L., and Matloff, G.L., "Solar Sails A Novel Approach to Interplanetary Travel, 2nd Edition," *Springer-Praxis Books in Space Exploration*, 2nd ed., Springer Science+Business Media, New York, 2015.
8. Walmsley, M., Heiligers, J., Ceriotti, M., and McInnes, C., "Optimal Trajectories for Planetary Pole-Sitter Missions," *Journal of Guidance, Control, and Dynamics, Under Review*; Vol., 2016
9. Battin, R.H., "An Introduction to the Mathematics and Methods of Astrodynamics, Revised Edition," *AIAA Eduction Series*, American Institute of Aeronautics and Astronautics, Inc., Reston, USA, 1999.
10. Brophy, J.R., Etters, M.A., Gates, J., Garner, C.E., Klatte, M., Lo, C.J., Marcucci, M.G., Mikes, S., Pixler, G., and Nakazono, B., "Development and Testing of the Dawn Ion Propulsion System," *42nd AIAA/ASME/SAE/ASEE Joint Propulsion Conference & Exhibit*, AIAA-2006-4319, Sacramento, USA, 2006.
11. Leiter, H.J., Killinger, R., Bassner, H., Müller, J., Kukies, R., and Fröhlich, T., "Development and Performance of the Advanced Radio Frequency Ion Thruster RIT-XT," *28th International Electric Propulsion Conference*, Toulouse, France, 2003.
12. Hutchins, M., Simpson, H., and Palencia Jiménez, J., "QinetiQ's T6 and T5 Ion Thruster Electric Propulsion System Architectures and Performances," *Joint Conference of 30th International Symposium on Space Technology and Science, 34th International Electric Propulsion Conference , and 6th Nano-satellite Symposium*, Hyogo-Kobe, Japan, 2015.
13. Heiligers, J., Diedrich, B., Derbes, B., and McInnes, C.R., "Sunjammer: Preliminary End-to-End Mission Design," *2014 AIAA/AAS Astrodynamics Specialist Conference*, San Diego, CA, USA, 2014.
14. Heiligers, J., Ceriotti, M., McInnes, C.R., and Biggs, J.D., "Mission Analysis and Systems Design of a Near-Term and Far-Term Pole-Sitter Mission," *Acta Astronautica*; Vol. 94, No. 1, 2014. doi: 10.1016/j.actaastro.2012.12.015
15. Leipold, M. and Götz, M., *Hybrid Photonic/Electric Propulsion*. 2002, Kayser-Threde GmbH, Technical Report SOL4-TR-KTH-001, ESA contract No. 15334/01/NL/PA: Munich, Germany.
16. Rao, A., "A Survey of Numerical Methods for Optimal Control," *Advances in the Astronautical Sciences*; Vol. 135, No. 1, 2009, pp. 497-528
17. Betts, J.T., "Survey of Numerical Methods for Trajectory Optimization," *Journal of Guidance, Control, and Dynamics*; Vol. 21, No. 2, 1998, pp. 193-207. doi: 10.2514/2.4231
18. Gautier, D.L., Bird, K.J., Charpentier, R.R., Grantz, A., Houseknecht, D.W., Klett, T.R., Moore, T.E., Pitman, J.K., Schenk, C.J., Schuenemeyer, J.H., Sørensen, K., Tennyson, M.E., Valin, Z.C., and C.J., W., "Assessment of Undiscovered Oil and Gas in the Arctic," *Science*; Vol. 324, No. 5931, 2009, pp. 1175-1179. doi: 10.1126/science.1169467
19. Fear, R.C., Milan, S.E., Carter, J.A., and Maggiolo, R., "The interaction between transpolar arcs and cusp spots," *Geophysical Research Letters*; Vol. 42, No. 22, 2015, pp. 9685-9693. doi: 10.1002/2015GL066194
20. McInnes, C.R. and Mulligan, P., "Final Report: Telecommunications and Earth Observations Applications for Polar Stationary Solar Sails." Report to the National Oceanic and Atmospheric Administration (NOAA) from the Deparment of Aerospace Engineering, University of Glasgow, 2003, pp. 1-51.
21. Raytheon, "Polesitter Telecom Experiment Study, Task 1 Results." Report to NOAA, 2004, pp. 1-140
22. Starchville, T.F., "Selected Results for Earth and Lunar Coverage from Artificial Lagrange Orbits," Report to NOAA. The Aerospace Corporation. NSF/OPP US Antarctic Program Satllite Comm., 2005.
23. National Science Foundation, "NOAA Bidders Conference, Solication NEEK-000-5-00274," 2005
24. Denig, W., "Point Paper: Utility of SESS Sensors on Polesitter Spacecraft. NPOESS SESS Goverenment Advisory Team," 2003.